ACS APPLIED MATERIALS & INTERFACES

Research Article

www.acsami.org

Microchannel Wetting for Controllable Patterning and Alignment of Silver Nanowire with High Resolution

Bo-Ru Yang,[†,‡] Wu Cao,[†] Gui-Shi Liu,[†] Hui-Jiuan Chen,[‡] Yong-Young Noh,[§] Takeo Minari,[∥] Hsiang-Chih Hsiao,[⊥] Chia-Yu Lee,[⊥] Han-Ping D. Shieh,[#] and Chuan Liu*[,†,‡]

[†]School of Microelectronics, School of Physics and Engineering, Guangdong Province Key Laboratory of Display Material and Technology, State Key Laboratory of Optoelectronic Materials and Technologies, Sun Yat-Sen University, Guangzhou 510275, People's Republic of China

[‡]SYSU-CMU Shunde International Joint Research Institute, Shunde 528000, People's Republic of China

[§]Department of Energy and Materials Engineering, Dongguk University, 26 Pil-dong, 3 ga, Jung-gu, Seoul 100-715, Republic of Korea

[∥]International Center for Materials Nanoarchitectonics (WPI-MANA), National Institute for Materials Science (NIMS), Tsukuba, Ibaraki 305-0044, Japan

[⊥]Shenzhen China Star Optoelectronics Technology Co., Ltd., Guangming New District No. 9-2, Tangming Road, Shenzhen 518132, People's Republic of China

[#]Department of Photonics/Display Institute, National Chiao Tung University, Hsinchu 300, Taiwan

Supporting Information

ABSTRACT: Patterning and alignment of conductive nanowires are essential for good electrical isolation and high conductivity in various applications. Herein a facile bottom-up, additive technique is developed to pattern and align silver nanowires (AgNWs) by manipulating wetting of dispersions in microchannels. By forming hydrophobic/hydrophilic micropatterns down to 8 μm with fluoropolymer (Cytop) and SiO_2, the aqueous AgNW dispersions with the optimized surface tension and viscosity self-assemble into microdroplets and then dry to form anisotropic AgNW networks. The alignment degree characterized by the full width at half-maximum (FWHM) can be well-controlled from 39.8° to 84.1° by changing the width of microchannels. A mechanism is proposed and validated by statistical analysis on AgNW alignment, and a static model is proposed to guide the patterning of general NWs. The alignment reduced well the electrical resistivity of AgNW networks by a factor of 5 because of the formation of efficient percolation path for carrier conduction.

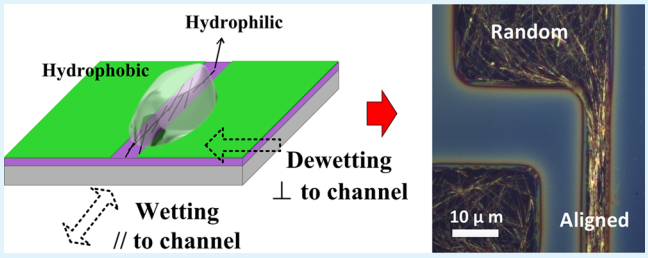

KEYWORDS: *fluoropolymer, microchannel, self-assembly patterning, alignment, silver nanowires*

1. INTRODUCTION

Significant progress has been made in novel one-dimensional (1D) nanostructures, such as inorganic or polymeric nanowires, nanoribbons, and nanotubes.[1−4] Especially, 1D silver nanowires (e.g., AgNWs), as novel conductive materials,[5,6] have attracted lots of attention for potential applications such as touch panels[7,8] and solar cells.[9−11] Yet challenges still exist for practical applications, e.g., precise patterning and control of orientations. Successful patterning of nanowires will significantly promote the device performance for excellent electrical isolation between adjacent devices, whereas sufficient alignment is vital for highly conductive, transparent films and nanoscale electronic devices.

For patterning techniques, a variety of top-down, subtractive methods have been developed, such as photolithography with wet chemical etching[12] and high energy density laser ablation.[13] However, the postetching process after film deposition and solvent contamination restricts their potentials. Besides, bottom-up methods[14−18] have also been developed, such as gravure printing,[14] ink jet printing,[15,16] polydimethylsiloxane (PDMS) stamp transferring,[17] and spray-coating with shadow mask.[18] However, the resolution of stamps and masks (usually larger than 20 μm) limits their applications in microelectronics. In general, bottom-up methods are superior to top-down ones in terms of streamlined processes, lower consumption of materials, and less destruction in films, which are preferred for large-scale printed electronics.

For alignment techniques, polymeric and inorganic 1D nanostructures have been reported, which extended rapidly to the assembly of two-dimensional (2D) and three-dimensional (3D) ordered nanostructures.[1] The anisotropic structure has been used by using the solid template,[19] chemically modified

Received: July 15, 2015
Accepted: September 4, 2015
Published: September 4, 2015

DOI: 10.1021/acsami.5b06370
ACS Appl. Mater. Interfaces 2015, 7, 21433−21441

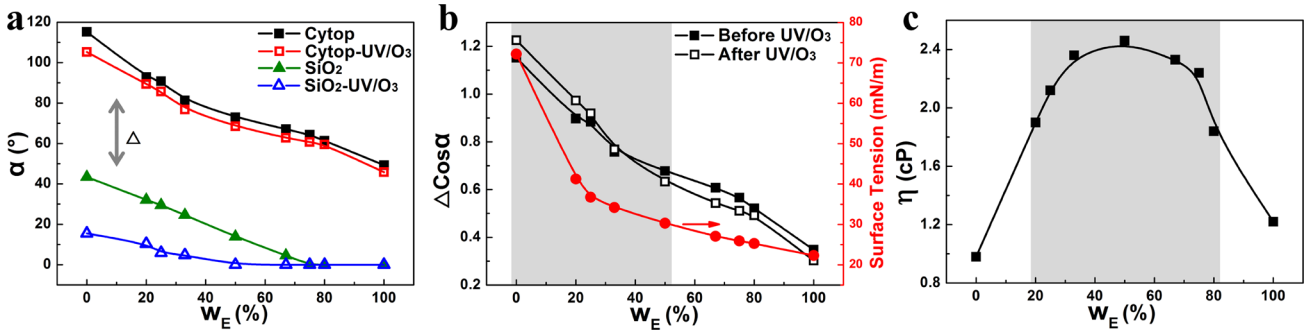

Figure 1. Properties of the mixed solvents (Eth:DI-H_2O) as a function of weight ratio of ethanol. (a) Contact angles on different substrates. $\Delta\alpha$ is the difference of contact angles on Cytop and SiO_2. (b) The difference value, $\Delta\cos\alpha = \cos\alpha(SiO_2) - \cos\alpha(\text{Cytop})$, and the measured surface tension. (c) Viscosity values at 20 °C. The gray squares in parts b and c represent the suitable range of w_E%, respectively.

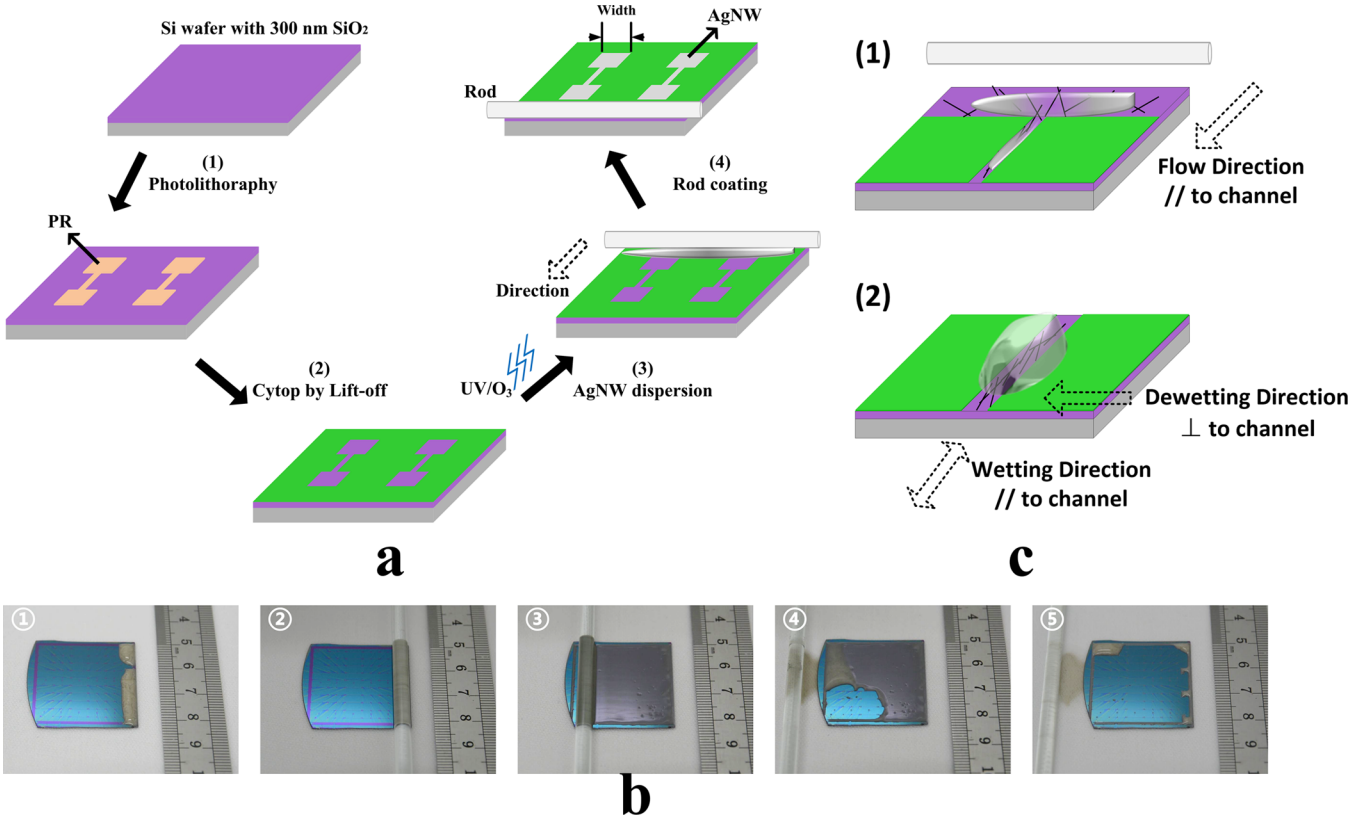

Figure 2. Patterning procedures. (a) Schematic representation of the fabrication process. (b) Captured photos at different times during rod coating step (extracted from Supporting Information movie S1). (c) The schematic diagrams of two possible microfluidic scenarios during dispersion-drying. The first one relies on rod-coating to align NWs, while the second one relies on surface tension.

surfaces,[20] Langmuir–Blodgett (L–B) method,[21] electromagnetic field assisted alignment,[3,22,23] and capillary flow in PDMS mold.[24] Yet for convenient and low cost applications, we still need to develop solution-processed techniques that are highly controllable in orientations of NWs and are compatible with conventional processes.

In this paper, we developed a bottom-up, additive strategy to simultaneously pattern and align the 1D AgNWs. The technology is based on surface engineering that forms micropatterns of fluoropolymer/SiO_2 surfaces and makes use of wetting/dewetting phenomena of fluid. The patterning achieved high resolution down to 8 μm and well-controlled the alignment by showing a full width at half-maximum (FWHM) from 39.8° to 84.1°. The quantitative investigations into the impact of microchannel width on AgNWs clarify the driving force and mechanism for the alignment. In the distribution of oriented angles, the aligned AgNWs networks exhibit 10 times higher peak-to-background ratio (39.5) as compared to those aligned by coating without patterning (4.3). Such strong anisotropic properties lead to a much reduced (5 times) electrical resistivity, which is very promising for functional electronics.

2. RESULTS AND DISCUSSION

Dispersion Properties. The patterning and alignment techniques developed are based on the self-assembly method by manipulating wettability, which has been previously explored for processing of other nanomaterials,[25−28] such as organic thin film transistors (OTFT)[25,26] and biomaterials.[28] The self-assembly of solution-processed patterning critically relies on

DOI: 10.1021/acsami.5b06370
ACS Appl. Mater. Interfaces 2015, 7, 21433−21441

two factors for the dispersion: (1) appropriate surface tension, and (2) stable dispersion and slow deposition of NWs. To obtain precise control and delicate balance of the two factors, we mixed deionized water (DI-H_2O, high polarity) and ethanol (Eth, low polarity) in different ratios. Figure 1a depicts the contact angle (α) of solvents with various weight ratio of Eth in solvent (w_E% ranges from 0 to 100%). To probe the effect on different surfaces, α was measured on hydrophobic Cytop and hydrophilic SiO_2 surfaces, respectively, and we also applied moderate surface treatment to remove the residual organics (6 min UV/O_3 treatment). On all the surfaces, α decreases as w_E% increases (e.g., α decreases from 115.2° to 49.3° on a bare Cytop surface), which signifies a decreased surface tension of the solvent as described by the Young equation[29,30]

$$\cos\alpha = \frac{\gamma^{SV} - \gamma^{SL}}{\gamma^{LV}} \quad (1)$$

Here, γ is interfacial tension at thermodynamic equilibrium, and S, L, V represent solid, liquid, and vapor, respectively. For reference, the surface tensions of the solvents range from 72 to 22 mN/m (Figure 1b, red dots), and the surface free energy of Cytop and SiO_2 is 20 mN/m and SiO_2 40.1 mN/m (literature values), respectively. Apparently, a large difference between the surface tensions is favored to enable good wetting/dewetting process on the Cytop/SiO_2 surfaces, manifested as large $\Delta\alpha$ or $\Delta\cos\alpha$.[31] Figure 1b illustrates that $\Delta\cos\alpha$ is almost inversely proportional to w_E%, decreasing from 1.20 to 0.32. The short-time UV/O_3 treatment cleaning SiO_2 surface further increased $\Delta\cos\alpha$ (or $\Delta\alpha$) when w_E% is smaller than 50%, and thus would help improve the patterning. Hence, w_E% should be between 0 and 50%, and UV/O_3 treatment should be performed for patterning the liquid-state dispersion.

To ensure the uniform dispersion of NWs during solvent drying, the viscosity η of solvents was studied by viscometer (at 20 °C), as shown in Figure 1c. The value of η increases from 0.98 cP at pure DI-H_2O to be 2.46 cP (maximum) when w_E% equals 50% and then decreases again to be 1.22 cP as w_E% reaches 100%. In general, small η leads to fast deposition and nonuniformity of NWs as the solvent evaporated easily and agglomerate, while relatively large η results in slower deposition during solvent drying to form uniform networks. We observed a low quality of the patterned AgNWs at a low ethanol concentration (w_E = 0) or at a higher w_E = 100%, due to a low viscosity and/or a low surface tension of dispersion. Hence, a value between 20% and 80% should be preferred for w_E% in order to have relatively stable dispersion during the solvent evaporation. Consequently, we shall keep w_E% within 20−50% as the optimum ratio.

Patterning Procedure. With the above results, we dispersed and ultrasonicated AgNWs in an Eth/DI-H_2O mixed solvent (Eth w_E% = 49.7%) with AgNW concentration of 0.3 wt %. The AgNWs were measured to have an average diameter of 125.7 nm and an average length (L_{NW}) of 19.8 μm (aspect ratio ~158, see Supporting Information, Figure S1). The patterning processes of AgNW are illustrated in Figure 2a. First, photoresist (PR) was patterned on a Si/SiO_2 substrate by photolithography. Then Cytop was spin-coated to form a thin layer (~50 nm, see Figure S2) on substrate followed by lift-off process and treated by UV/O_3 as described above. The corresponding optical image and contact angle measurement of Cytop are shown as Figure S3. The Cytop patterns gap the SiO_2 long microchannels with the channel width (W) from 8 to 50 μm, and each microchannel connects two square patterns to improve lift-off quality. Finally, the dispersion of AgNWs was coated by rolling a glass rod on the substrate, and the density of NW network can be controlled by changing the coating times. The final step including the rod-coating and the motion of liquid are shown by optical images in Figure 2b, and a full video in movie S1. The aqueous AgNWs dispersion was first covered on the whole substrate (Figure 2b, part 3), then promptly dewet from the Cytop surface, and finally only deposited on the exposed SiO_2 area (Figure 2b, parts 4 and 5).

Scenario of Alignment. According to the above macroscopic observations, we propose that two following microfluidic scenarios may occur during dispersion-drying, both of which would lead to significant alignment of AgNWs: (1) The coating rod affords the shearing force to the AgNWs which anchor the substrate and orient parallel to the coating direction (Figure 2c, part 1). This is similar to the cases in alignment processed by Meyer-rod coating.[32] In this scenario, AgNWs align mainly in the microchannel parallel to the coating direction, regardless of the value of channel width W. We refer to it as the "shearing alignment". (2) The different surface tensions of the surrounding hydrophobic Cytop and the defined hydrophilic SiO_2 surface drive the AgNWs dispersion to shrink into microchannels of SiO_2, forming long stick-shaped microdrops. The microdrops align the AgNWs to follow the shape of microchannel with a large aspect ratio. In this scenario, AgNWs align in the microchannels regardless of the directions, but result in better aligned when the value of W is small (Figure 2c, part 2). We refer to it as the "microchannel wetting alignment". In the following, we examine the morphology of AgNWs and investigate which scenario is dominant in our experiments.

Patterning Results. The patterned AgNWs were characterized by scanning electron microscope (SEM) and polarizing optical microscope (POM), as shown in Figure 3. The SEM image illustrates that the AgNWs were precisely patterned into the microchannels down to 8 μm, and the AgNWs were well-aligned following the direction of the microchannels. The OM images also illustrate good uniaxial orientation of the AgNWs bunches with anisotropic features (Figure 3b,c). It is worth

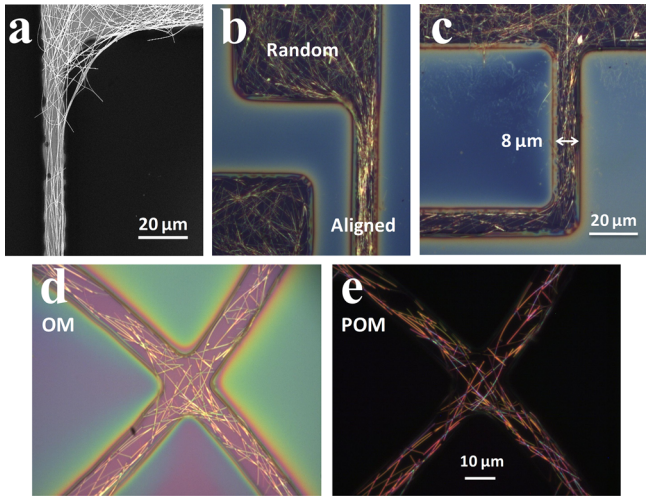

Figure 3. (a) SEM image of aligned AgNWs. (b) OM image of a transition region from randomly distributed to aligned AgNWs. (c) OM image of AgNWs aligned in a channel with a 90°corner. (d) OM and (e) POM images of AgNWs aligned in two orthogonal microchannels.

DOI: 10.1021/acsami.5b06370
ACS Appl. Mater. Interfaces 2015, 7, 21433−21441

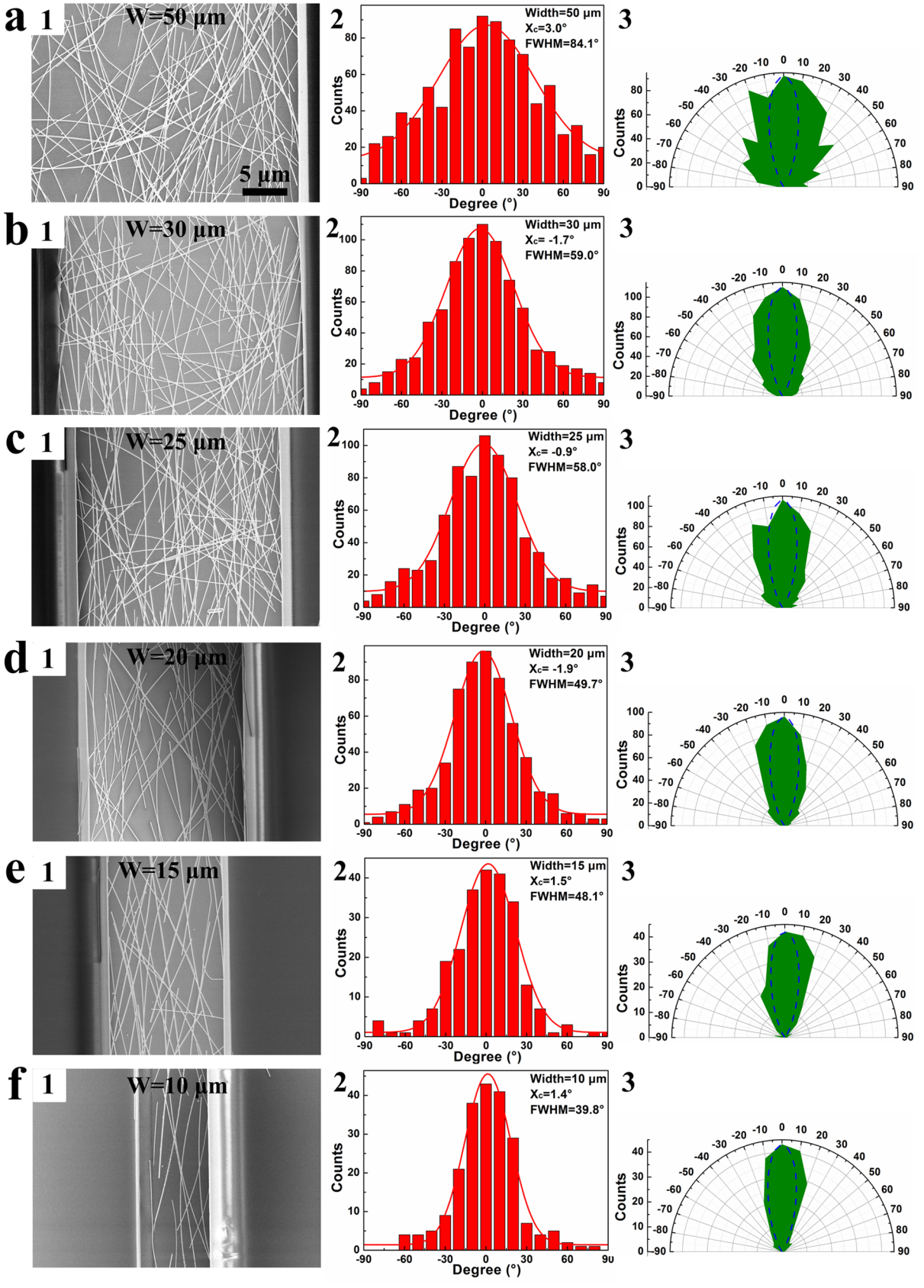

Figure 4. Characterization of AgNWs in microchannels with SEM images (the left column), histograms of oriented angles of nanowires (the middle column), and polar diagrams (the right column): W = 50 (a), 30 (b), 25 (c), 20 (d), 15 (e), and 10 (f) μm. The dashed curves in polar diagrams represent the Gaussian distribution with X_c at 0° and FWHM of 30°.

DOI: 10.1021/acsami.5b06370
ACS Appl. Mater. Interfaces 2015, 7, 21433−21441

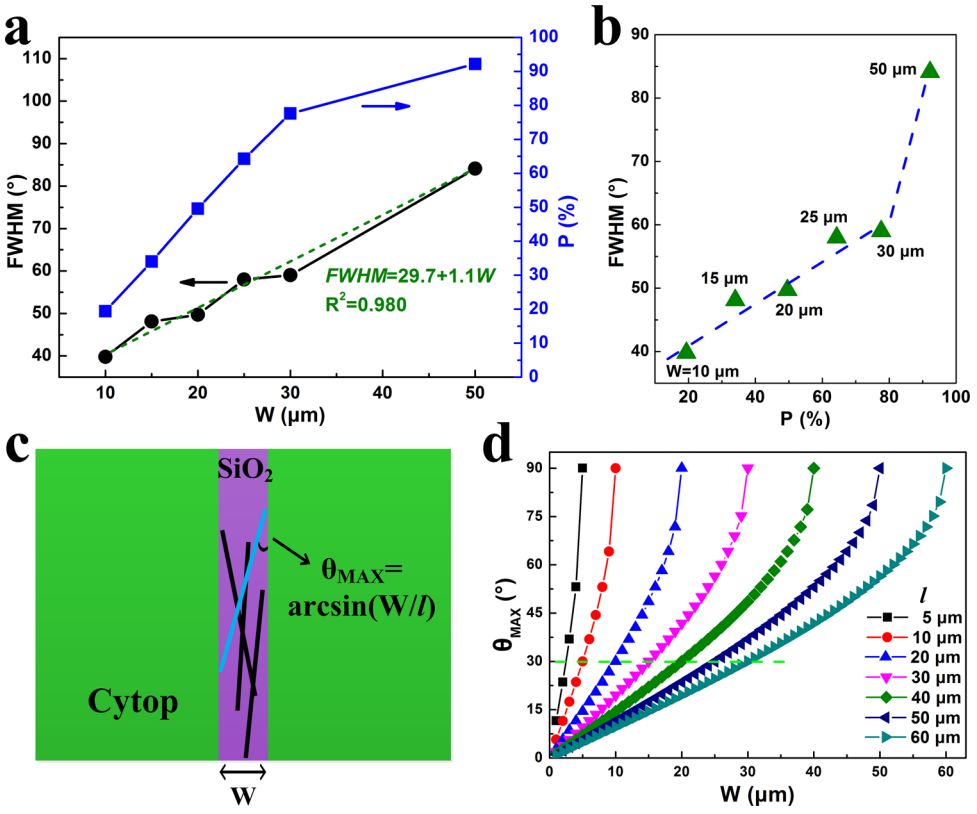

Figure 5. (a) Relationship between channel width (W), short nanowire percent (P%), and FWHM. Dashed line is obtained from a linear fitting. (b) The relationship between P% and FWHM. (c) Static model used for estimating the proper channel width for the alignment. (d) The relationship between W and θ_{MAX}. Dashed line corresponds to θ_{MAX} of 30°.

mentioning that the surrounding Cytop can be dissolved by perfluorinated solvent without deteriorating nanowires for further investigations and applications (Figure S4). At the connecting area between the microchannel and large square, there is a clear transition of AgNWs from being randomly oriented to being well-aligned. To examine the relation between the rod-coating direction and the alignment, we fabricated orthogonally oriented microchannels (W = 10 μm) and found that AgNWs are well-located and aligned in both arms of the cross (Figure 3d,e). Such results indicate that the alignment does not rely on the coating direction and support the "microchannel wetting alignment" as proposed above, wherein the driving force of the self-assembled alignment is the different surface tensions in/out of the microchannels.

Mechanism Study. To further investigate the alignment effect, we fabricated microchannels with various W of 10, 15, 20, 25, 30, and 50 μm on one substrate. The smallest W = 10 μm is shorter than that of (L_{NW} = 19.8 μm) most AgNWs, while the largest W = 50 μm is longer than that of most AgNWs (cf., Figure S1b). After coating the rods for three times, the samples are characterized with SEM (Figure 4, the left column). Qualitatively, the AgNWs are better aligned along the channel direction when W is small (below 15 μm), as compared to the wider channels (W reaches 30 μm) where a significant proportion of nanowires becomes randomly oriented. A quantitative and statistic study is performed by giving the histogram of the oriented angle of individual AgNWs (Figure 4, the middle column). Gaussian fittings are applied to derive the center degree (X_c) and full width at half-maximum (FWHM). The FWHM characterizes the deviation in orientations relative to the microchannel direction,[33,34] and is used to define the extent of alignment here: AgNWs are considered perfectly aligned (anisotropic) as FWHM is 0°, while AgNWs become more randomly oriented (isotropic) as *FWHM* increases toward 180°. As W decreases from 50 to 10 μm, FWHM decreases from 84.1° to 39.8°. To better visualize the distribution of orientations, we plot the histograms into polar diagrams (Figure 4, the right column) and, for a reference, plot an ideal Gaussian distribution with X_c at 0° and FWHM of 30° (dashed curves). From 50 to 10 μm microchannel, the distribution of orientation angles starts from being a rather wide, radiative shape and then gradually becomes a narrow, ellipse-shape distribution, close to the ideal distribution (dashed curves). In addition, the narrow microchannels exhibit many fewer counts near 90°, coming from totally nonaligned NWs. These results clearly support the "microchannel wetting alignment" and demonstrate the importance of small W.

Only NWs longer than the channel width ($l > W$) are confined and aligned. In other words, NWs that are shorter than W ($l < W$) will be randomly oriented and thus increase the value of FWHM. The proportion of them is calculated by integrated area ratio:

$$P\% = \frac{S(l < W)}{S} \quad (2)$$

Here, the S refers to the total area, and $S(l < W)$ refers to the area where the NWs length are smaller than W (cf., the fitting curve in Figure S1b). Then we are able to probe the relationship between the W, FWHM, and P% as depicted in Figure 5a,b. The value of FWHM increases (signifying weaker alignment effect) almost linearly with P% from 20% to 78% (corresponding to W = 10−30 μm), and then suddenly jumped

DOI: 10.1021/acsami.5b06370
ACS Appl. Mater. Interfaces 2015, 7, 21433−21441

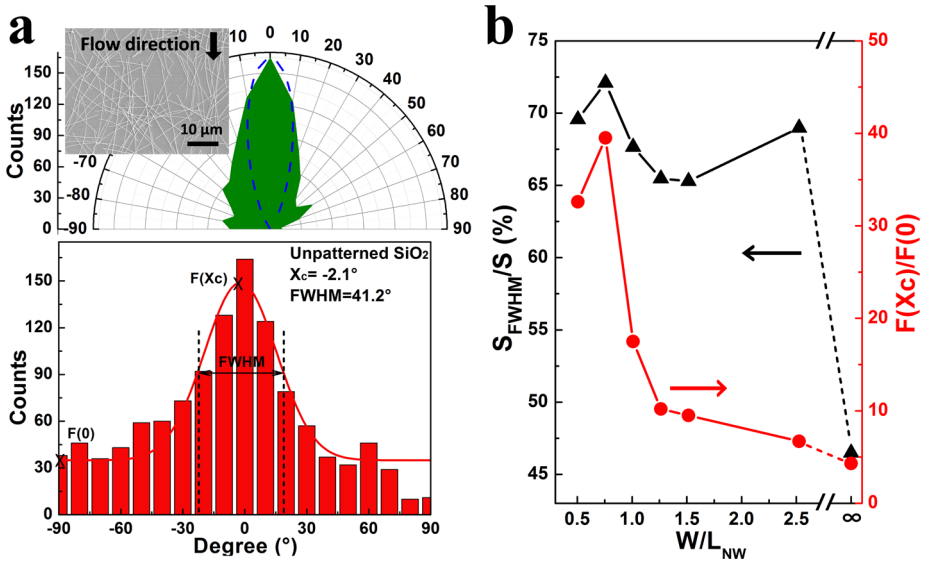

Figure 6. (a) Polar diagram (up) and histogram (down) of angle distribution on an unpatterned sample. Inset: SEM image of coated AgNWs. (b) The relationships between W/L_{NW} and integrated area ratio (S_{FWHM}/S), and the dimensionless parameter $[F(X_c)/F(0)]$.

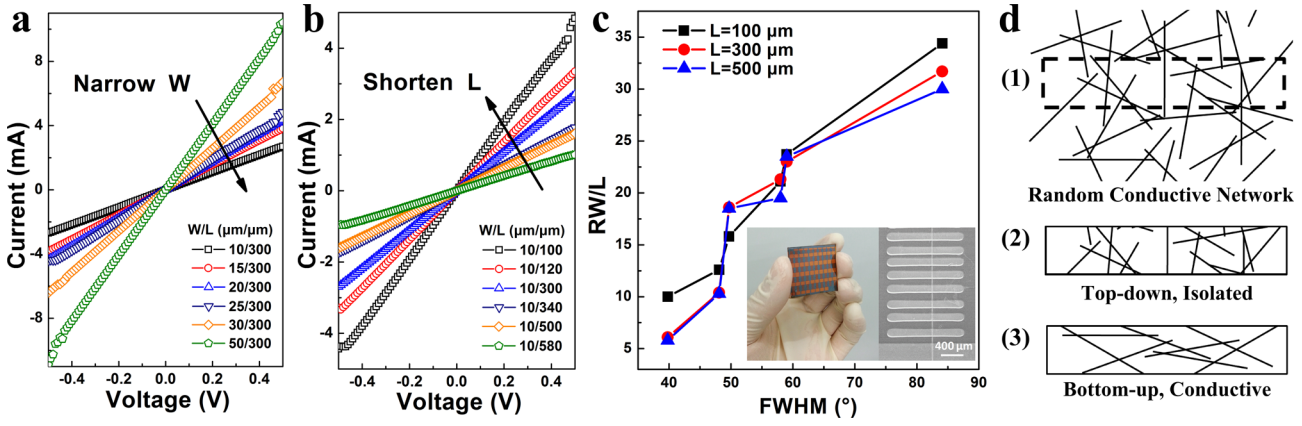

Figure 7. (a) I/V sweep curves when changing W. (b) The I/V sweep curves when changing L. (c) The relationship between the normalized RW/L and FWHM. Inset is a sample deposited with electrode. (d) Schematic diagrams for indicating the superiorities of the proposed bottom-up process.

when P% is 92% (W = 50 μm). The results agree well with the proposed mechanism and indicate that the ratio between l and W is the key to achieve good alignment. Yet, what value of W is needed to guarantee sufficient alignment? We further put forward an ideal, static model by assuming rigid NWs as shown in Figure 5c, where all NWs of l in length are confined and randomly distributed in a microchannel. Then, the maximum angle between the NWs and edge of microchannel, θ_{MAX}, is simply given by

$$\theta_{MAX} = \arcsin\left(\frac{W}{l}\right) \tag{3}$$

We used eq 3 to simulate the obtained θ_{MAX} as a function of W as shown in Figure 5d. If algining NWs within the orientation angle of θ_{MAX} = 30°, then we shall fabricate the microchannels with the proper width (W_0):

$$W_0 \leq \frac{l}{2} \sim \frac{L_{NW}}{2} \tag{4}$$

Then, in experiments, we can simply use the meausred L_{NW} to estimate the microchannel width for patterning and aligning of NWs.

Comparing Two Alignments. The microchannel wetting alignment is compared with the rod coating on a 2 cm × 2 cm unpatterned SiO_2/Si substrate, of which the SEM image, histogram of oriented angles, and polar diagram are shown in Figure 6a. A relatively small FWHM of 41.2° is obtained by Gaussian fitting, indicating a certain degree of alignment was achieved on a nonpatterned surface. As the substrate size is much larger than W, we consider the channel width W here as infinity (∞) when comparing with microchannels. However, we notice that, in the polar diagram, large counts were obtained near 90°, and in the histogram, the baseline of Gaussian fitting is significantly larger than zero. To quantitatively describe such features, we introduce two other parameters: the peak to baseline ratio, i.e., $F(X_c)/F(0)$, and the area ratio S_{FWHM}/S, i.e., the ratio between area within FWHM and total area (illustrated in Figure 6a). Values of the two parameters are compared in Figure 6b and Table S1. Both parameters generally decrease with W/L_{NW} and reach their minima in the unpatterned case, signifying the lower quality of alignment. Therefore, a microchannel wetting alignment provides more precise patterning and avoids scratching the surface of substrate that may occur during rod-coating without patterning. In addition,

DOI: 10.1021/acsami.5b06370
ACS Appl. Mater. Interfaces 2015, 7, 21433−21441

we propose that the two parameters $[S_{FWHM}/S$ and $F(X_c)/F(0)]$, in addition to FWHM, should be considered when characterizing the degree of alignment of 1D nanomaterials.

Electrical Performance. To investigate the impact of alignment on the electrical performance of AgNW networks like other 1D materials,[34−36] we applied the above technique followed by metal deposition (Au/Al) to form electrode contacts. The channel length (L) between electrodes varies from 100 to 500 μm which is far above the average length of AgNWs. The current−voltage ($I-V$) sweep curves were measured on AgNWs (without annealing) by a semiconductor parameter analyzer for different W and L as plotted in Figure 7a,b. For comparisons, the extracted total resistances (R's) are normalized in RW/L (Figure 7c), which monotonically increases from 6.1 to 31.7 as a function of FWHM, implying that the conductivity of the AgNWs networks is enhanced by a higher alignment degree. The above finding indicates that the aligned and anisotropic NWs form more or shorter percolated pathways than the unaligned and isotropic NWs. Moreover, according to the percolation theory of 1D conducting materials, the above results indicate that our alignment did not reduce wire−wire connections, which were observed in carbon nanotubes aligned by melt fiber spinning.[35] The detailed transport mechanisms of NWs with large aspect ratio will be studied in a future work.

Finally, the above bottom-up, additive patterning technology is compared with the top-down, subtractive patterning in Figure 7d, which illustrates a certain number of 1D NWs with the same length that are patterned by the two different processes. The randomly distributed NWs that were subtractive patterned into strips (e.g., by wet etching) became isolated wires, so that it requires a large density of materials to form a conductive pathway. On the contrary, in the bottom-up, additive patterning (i.e., microchannel wetting alignment), even fewer NWs provide a conductive pathway in the stripe of the same size. In another word, the presented technique exhibits advantages in providing precise patterning, high conductivity, and less destruction in networks.

3. CONCLUSION

We developed a bottom-up, additive technique to pattern and align 1D metal nanowires (e.g., AgNWs). By delicate control of the solvent components, surface conditions, and coating procedures, AgNWs were confined in microchannels with resolution down to 8 μm with a considerably high degree of alignment. Morphological and statistic study on the AgNWs indicates that the different surface tension is the driving force for the alignment, and the narrow channel gapped by the hydrophobic surrounding surface is the key for forming long stick-shape microdroplets and for controlling FWHM in the distribution of oriented angles. Accordingly, we propose that, for sufficient alignment, the proper channel width shall satisfy $W_0 \leq L_{NW}/2$.

Compared to alignment by contact-mode rod-coating without patterning, the presented techniques exhibit better anisotropic properties of high peak-to-background ratios. Moreover, electrical characterization on the AgNWs networks indicates that better alignment (i.e., small FWHM) sufficiently lowers the total resistance, implying a more efficient conductive path. This facile, additive, solution-processed technique is compatible with conventional patterning processes, a promising strategy in organizing various 1D building blocks into functional electronic devices.

4. METHODS

Dispersion Preparations and Characterizations. AgNWs (Blue Nano Inc.) dispersed in ethanol with concentration of 1.25 wt % was ultrasonicated in aqueous solvent (Eth w_E% = 33.3%) at a weight ratio of 1:3, reaching a final AgNWs weight ratio of 0.3 wt %. The density of the network can be controlled by changing the coating times or AgNW weight ratio in dispersion. Contact angle (α) and surface tension were measured via contact angle meter (Dataphysics, OCA15), and viscosity values were obtained from a viscometer (Brookfield, DV2T), respectively.

Surface Prepatterning and Characterizations. Cytop (CTL-809M) and specific perfluorinated solvent (CT-Solv 180) were purchased from Asahi Glass Corp. In order to use a lift-off process, thick photoresist was spun on a thermally grown 300 nm-thick SiO_2/Si wafer and patterned by the photolithography. A diluted Cytop solution (3.33 wt %) was then spun over the substrate with photoresist patterns at 5000 rpm, followed by annealing for 15 min at 150 °C in air. Lift-off process was carried out using acetone and sonication. The thickness of Cytop was measured to be around 50 nm via SEM (Hitachi, S-4800) as shown in Supporting Information (Figure S2). Before the rod coating procedure, a 6 min UV/O_3 treatment (SEN, PL17-110) was needed for better performance.

AgNW Coating and Characterizations. The AgNW ink was coated on the substrate using a glass rod in one direction, and the density of the network can be controlled by changing the coating times. A fabricated sample with different channels was characterized under the SEM, to identify the alignment effect; the images were used to calculate the angle deviation from long axis of nanowire to channel direction by a self-compiled software via Matlab (Figure S5). Gaussian curves could be obtained after fitting, and consequently, the extracted FWHM values could represent the orientation scatter or the alignment degree.

Electrical Characterizations. The 40 nm-thick Au and 100 nm-thick Al electrodes were evaporated in turn onto the AgNW deposited samples with a metal shadow mask. The distances between two electrodes varied from 100 to 500 μm which were far above the average length of AgNWs. Electrical performance measurements of the aligned AgNWs networks in different channel regions were then implemented via a semiconductor parameter analyzer (Agilent, B1500A).

■ ASSOCIATED CONTENT

Supporting Information

The Supporting Information is available free of charge on the ACS Publications website at DOI: 10.1021/acsami.5b06370.

Detailed description of the materials used in the experiments (PDF)

Movie showing final steps of patterning process (AVI)

■ AUTHOR INFORMATION

Corresponding Author

*E-mail: liuchuan5@sysu.edu.cn.

Author Contributions

The manuscript was written through contributions of all authors. All authors have given approval to the final version of the manuscript.

DOI: 10.1021/acsami.5b06370
ACS Appl. Mater. Interfaces 2015, 7, 21433−21441

Notes

The authors declare no competing financial interest.

■ ACKNOWLEDGMENTS

This work was financially supported by the projects from the National Natural Science Foundation of China (Grant 61307027), the Key Construction of the National "985" Project (30000-31101200), the National High Technology Research and Development Program of China (863 Project) (2015AA033408), and the Science and Technology Program of Guangdong Province (2014-B090914001). The project was partially supported by the Shunde Government, Guangdong Province, China, under Contract 20140401.

■ ABBREVIATIONS

AgNWs, silver nanowires
NWs, nanowires
PDMS, polydimethylsiloxane
OTFT, organic thin film transistors
DI-H_2O, deionized water
Eth, ethanol
α, contact angle
η, viscosity
w_E%, weight ratio of Eth in solvent
L_{NW}, average length of AgNW
PR, photoresist
W, channel width
SEM, scanning electron microscopy
POM, polarizing optical microscope
FWHM, full width at half-maximum
l, length of individual AgNW
P%, percent of nanowires which are longer than channel width ($l < W$)
θ_{MAX}, maximum angle between the NWs and microchannel
S_{FWHM}/S, ratio between the area within FWHM and the total area
$F(X_c)/F(0)$, peak value to baseline value ratio
L, channel length between electrodes

■ REFERENCES

(1) Su, B.; Wu, Y.; Jiang, L. The Art of Aligning One-Dimensional (1D) Nanostructures. *Chem. Soc. Rev.* **2012**, *41*, 7832−7856.
(2) Ye, S.; Rathmell, A. R.; Chen, Z.; Stewart, I. E.; Wiley, B. J. Metal Nanowire Networks: the Next Generation of Transparent Conductors. *Adv. Mater.* **2014**, *26*, 6670−6687.
(3) Li, D.; Wang, Y.; Xia, Y. Electrospinning Nanofibers as Uniaxially Aligned Arrays and Layer-byLayer Stacked Films. *Adv. Mater.* **2004**, *16*, 361−366.
(4) Xiang, R.; Yang, Z.; Zhang, Q.; Luo, G.; Qian, W.; Wei, F.; Kadowaki, M.; Einarsson, E.; Maruyama, S. Growth Deceleration of Vertically Aligned Carbon Nanotube Arrays Catalyst Deactivation or Feedstock Diffusion Controlled? *J. Phys. Chem. C* **2008**, *112*, 4892−4896.
(5) De, S.; Higgins, T. M.; Lyons, P. E.; Doherty, E. M.; Nirmalraj, P. N.; Blau, W. J.; Boland, J. J.; Coleman, J. N. Silver Nanowire Networks as Flexible, Transparent, Conducting Films Extremely High DC to Optical Conductivity Ratios. *ACS Nano* **2009**, *3*, 1767−1774.
(6) Akter, T.; Kim, W. S. Reversibly Stretchable Transparent Conductive Coatings of Spray-Deposited Silver Nanowires. *ACS Appl. Mater. Interfaces* **2012**, *4*, 1855−1859.
(7) Lee, J.; Lee, P.; Lee, H.; Lee, D.; Lee, S. S.; Ko, S. H. Very Long Ag Nanowire Synthesis and its Application in a Highly Transparent, Conductive and Flexible Metal Electrode Touch Panel. *Nanoscale* **2012**, *4*, 6408−6414.
(8) Madaria, A. R.; Kumar, A.; Zhou, C. Large Scale, Highly Conductive and Patterned Transparent Films of Silver Nanowires on Arbitrary Substrates and their Application in Touch Screens. *Nanotechnology* **2011**, *22*, 245201.
(9) Yang, L.; Zhang, T.; Zhou, H.; Price, S. C.; Wiley, B. J.; You, W. Solution-Processed Flexible Polymer Solar Cells with Silver Nanowire Electrodes. *ACS Appl. Mater. Interfaces* **2011**, *3*, 4075−4084.
(10) Chen, T. G.; Huang, B. Y.; Liu, H. W.; Huang, Y. Y.; Pan, H. T.; Meng, H. F.; Yu, P. Flexible Silver Nanowire Meshes for High-Efficiency Microtextured Organic-Silicon Hybrid Photovoltaics. *ACS Appl. Mater. Interfaces* **2012**, *4*, 6857−6864.
(11) Song, M.; You, D. S.; Lim, K.; Park, S.; Jung, S.; Kim, C. S.; Kim, D. H.; Kim, D. G.; Kim, J. K.; Park, J.; Kang, Y. C.; Heo, J.; Jin, S. H.; Park, J. H.; Kang, J. W. Highly Efficient and Bendable Organic Solar Cells with Solution-Processed Silver Nanowire Electrodes. *Adv. Funct. Mater.* **2013**, *23*, 4177−4184.
(12) Kim, S.; Kim, S. Y.; Kim, J.; Kim, J. H. Highly Reliable AgNW-PEDOT:PSS Hybrid Films: Efficient Methods for Enhancing Transparency and Lowering Resistance and Haziness. *J. Mater. Chem. C* **2014**, *2*, 5636−5643.
(13) Henley, S. J.; Cann, M.; Jurewicz, I.; Dalton, A.; Milne, D. Laser Patterning of Transparent Conductive Metal Nanowire Coatings: Simulation and Experiment. *Nanoscale* **2014**, *6*, 946−952.
(14) Park, J. D.; Lim, S.; Kim, H. Patterned Silver Nanowires using the Gravure Printing Process for Flexible Applications. *Thin Solid Films* **2015**, *586*, 70−75.
(15) Finn, D. J.; Lotya, M.; Coleman, J. N. Inkjet Printing of Silver Nanowire Networks. *ACS Appl. Mater. Interfaces* **2015**, *7*, 9254−9261.
(16) Minemawari, H.; Yamada, T.; Matsui, H.; Tsutsumi, J.; Haas, S.; Chiba, R.; Kumai, R.; Hasegawa, T. Inkjet Printing of Single-Crystal Films. *Nature* **2011**, *475*, 364−367.
(17) Xu, F.; Zhu, Y. Highly Conductive and Stretchable Silver Nanowire Conductors. *Adv. Mater.* **2012**, *24*, 5117−5122.
(18) Madaria, A. R.; Kumar, A.; Ishikawa, F. N.; Zhou, C. Uniform, Highly Conductive, and Patterned Transparent Films of a Percolating Silver Nanowire Network on Rigid and Flexible Substrates using a Dry Transfer Technique. *Nano Res.* **2010**, *3*, 564−573.
(19) Li, L.; Koshizaki, N.; Li, G. Nanotube Arrays in Porous Anodic Alumina Membranes. *J. Mater. Sci. Technol.* **2008**, *24*, 550−562.
(20) Burghard, M.; Duesberg, G.; Philipp, G.; Muster, J.; Roth, S. Controlled Adsorption of Carbon Nanotubes on Chemically Modified Electrode Arrays. *Adv. Mater.* **1998**, *10*, 584−588.
(21) Tao, A.; Kim, F.; Hess, C.; Goldberger, J.; He, R.; Sun, Y.; Xia, Y.; Yang, P. Langmuir-Blodgtt Silver Nanowire Monolayers for Molecular Sensing using Surface-Enhanced Raman Spectroscopy. *Nano Lett.* **2003**, *3*, 1229−1233.
(22) Lynch, M. D.; Patrick, D. L. Organizing Carbon Nanotubes with Liquid Crystals. *Nano Lett.* **2002**, *2*, 1197−1201.
(23) Cao, Y.; Liu, W.; Sun, J.; Han, Y.; Zhang, J.; Liu, S.; Sun, H.; Guo, J. A Technique for Controlling the Alignment of Silver Nanowires with an Electric Field. *Nanotechnology* **2006**, *17*, 2378−2380.
(24) Huang, Y.; Duan, X.; Wei, Q.; Lieber, C. M. Directed Assembly of One-Dimensional Nanostructures into Functional Networks. *Science* **2001**, *291*, 630−633.
(25) Kumatani, A.; Liu, C.; Li, Y.; Darmawan, P.; Takimiya, K.; Minari, T.; Tsukagoshi, K. Solution-Processed, Self-Organized Organic Single Crystal Arrays with Controlled Crystal Orientation. *Sci. Rep.* **2012**, *2*, 393.
(26) Kim, S. H.; Choi, D.; Chung, D. S.; Yang, C.; Jang, J.; Park, C. E.; Park, S. H. K. High-Performance Solution-Processed Triisopropylsilylethynyl Pentacene Transistors and Inverters Fabricated by using the Selective Self-Organization Technique. *Appl. Phys. Lett.* **2008**, *93*, 113306.
(27) Chabinyc, M. L.; Wong, W. S.; Salleo, A.; Paul, K. E.; Street, R. A. Organic Polymeric Thin-Film Transistors Fabricated by Selective Dewetting. *Appl. Phys. Lett.* **2002**, *81*, 4260.

DOI: 10.1021/acsami.5b06370
ACS Appl. Mater. Interfaces 2015, 7, 21433−21441

(28) Lee, C. S.; Lee, S. H.; Park, S. S.; Kim, Y. K.; Kim, B. G. Protein Patterning on Silicon-Based Surface using Background Hydrophobic Thin Film. *Biosens. Bioelectron.* **2003**, *18*, 437−444.
(29) Lenz, P. Wetting Phenomena on Structured Surfaces. *Adv. Mater.* **1999**, *11*, 1531−1534.
(30) Checco, A.; Guenoun, P.; Daillant, J. Nonlinear Dependence of the Contact Angle of Nanodroplets on Contact Line Curvature. *Phys. Rev. Lett.* **2003**, *91*, 186101.
(31) Matsui, H.; Noda, Y.; Hasegawa, T. Hybrid Energy-Minimization Simulation of Equilibrium Droplet Shapes on Hydrophilic/Hydrophobic Patterned Surfaces. *Langmuir* **2012**, *28*, 15450−15453.
(32) Zhu, S.; Gao, Y.; Hu, B.; Li, J.; Su, J.; Fan, Z.; Zhou, J. Transferable Self-Welding Silver Nanowire Network as High Performance Transparent Flexible Electrode. *Nanotechnology* **2013**, *24*, 335202.
(33) Wang, Y.; Pillai, S. K. R.; Chan-Park, M. B. High-Performance Partially Aligned Semiconductive Single-Walled Carbon Nanotube Transistors Achieved with a Parallel Technique. *Small* **2013**, *9*, 2960−2969.
(34) White, S. I.; DiDonna, B. A.; Mu, M.; Lubensky, T. C.; Winey, K. I. Simulations and Electrical Conductivity of Percolated Networks of Finite Rods with Various Degrees of Axial Alignment. *Phys. Rev. B: Condens. Matter Mater. Phys.* **2009**, *79*, 024301.
(35) Du, F.; Fischer, J. E.; Winey, K. I. Effect of Nanotube Alignment on Percolation Conductivity in Carbon Nanotube/Polymer Composites. *Phys. Rev. B: Condens. Matter Mater. Phys.* **2005**, *72*, 121404.
(36) Li, B.; Zhang, Y. C.; Li, Z. M.; Li, S. N.; Zhang, X. N. Easy Fabrication and Resistivity-Temperature Behavior of an Anisotropically Conductive Carbon Nanotube−Polymer Composite. *J. Phys. Chem. B* **2010**, *114*, 689−696.

DOI: 10.1021/acsami.5b06370
ACS Appl. Mater. Interfaces 2015, 7, 21433−21441